Role of gas bubbles in the attenuation of acoustic waves at the air–sea interface

Prasad K. Bhaskaran*

Department of Ocean Engineering and Naval Architecture, Indian Institute of Technology, Kharagpur 721 302, India

Gas bubbles produced by breaking waves play an important role in acoustic sound transmission. For a wide range of frequencies, the scattering is resonant in nature, and resonant bubbles scatter as well as absorb acoustic energy changing the compressibility of seawater. The present study deals with gas bubbles at the air–sea interface and their role in the attenuation and scattering of underwater sound propagation. This study leads to development of a damping model for gas bubbles as function of their size and acoustic frequency, including their role at resonance frequency covering aspects on damping mechanism due to thermal, viscous and radiation effects. The damping model estimates the variation of attenuation rate at resonance frequency for high wind speeds utilizing input from bubble population model considering geometrical aspects, and parameterizes bubble distribution at different stages of evolution. The study also estimates attenuation of sound speed in the presence of bubbles using climatology fields from the World Ocean Atlas. Finally, to assess the behaviour of random bubbles on sound attenuation, the statistical distribution function signifies that damping characteristics follows a normal distribution.

Keywords: Air–sea interface, attenuation, damping, gas bubbles.

GAS bubbles resulting from breaking ocean waves have significant impact in enhancing gas transfer at the air–sea interface, production of marine aerosols, forage biological surfactants, optical scattering and actively contribute to ambient noise in the ocean. However, direct measurement of early bubble population in the ocean is a highly challenging task. The variety of mechanisms involved in generation of oceanic bubbles includes action of surface wave breaking, dynamic interaction of rain on water waves, and many others. Based on experimental evidences, under moderate wind condition most of bubbles near ocean surface are due to breaking waves. The early attempts to measure bubble population involved methods based on bubble traps, acoustics and photography. The bubble trap method[1] provided a means to capture the bubbles, with a limitation that each measurement had a delay time for the smallest bubble to rise to the surface. Therefore, the cumulative effect due to bubble dissolution, growth and coalescence using this method was questionable. The acoustic method[2] had difficulties in data interpretation due to large bubble concentrations observed at low wind-speed conditions, thereby leading to the photographic method[3]. In a historical perspective, the earliest oceanic bubble population measurements in 20–30 m water depths used sophisticated optical measurement technique[3]. The study noticed for near-surface (0.7 m) waters and for wind speed between 11 and 13 m s^{-1}, a steady increase in bubble population for size between approximately 200 and 60 μm radii[3]. However, the photographic observations lack necessary resolution to observe smaller bubbles, and measured population in general may underestimate the actual population[4]. The acoustic technique[5] used four upward-looking sonar transducers that monitored linear backscatter at four frequencies, viz. 28, 50, 88 and 200 kHz. This data inferred the ambient bubble population to model the waveguide propagation characteristics in bubbly oceanic environment. Another notable historical measurement used a flat plate resonator to characterize oceanic bubble population[6]. This technique assumes linear bubble behaviour that affects mode attenuation set-up between two resonator plates, used to infer bubble population at model frequencies. This experiment was conducted near surface (≈25 cm) at 12 m s^{-1} wind speed and 120 m water depth. The results showed a monotonic increase in bubble population between 250 and 30 μm, with a high number of larger bubbles and slightly reduced number of smaller bubbles[5]. Another study used the acoustic resonator with a larger radius span[7] compared to the historical measurement[6]. The results[7] showed good agreement for bubble size larger than 40 μm, including smaller bubble[3,6]. One can find a concise treatment on the interaction of acoustic field with bubbles in Leighton[8].

Another technique used a combination frequency measurement, sizing bubbles in the laboratory using sophisticated signal processing techniques[9–11] and bubble population[12]. It utilized a chirped signal as the pump source at an imaging frequency of 450 kHz. The combination frequency technique measured population in the surf zone at water depths of 1.5 m for pump frequencies of 28, 50, 60 and 88 kHz using the calibration technique[13]. In addition, a buoy-deployed combination frequency acoustic technique[14] measured near-surface

*e-mail: pkbhaskaran@naval.iitkgp.ernet.in

bubble population in the open sea. Six trials were performed over a one-day period comprising ten snapshots for local bubble population at ten discrete radii[14]. A recent work[15] used optical measurements of small, deeply penetrating bubble populations generated by breaking waves in the Southern Ocean. This study used optical measurement for bubble size distribution (ranging from 0.5 to 125 μm radius) during high wind speeds (≈13 m s^{-1}) under large-scale wave breaking[15]. The study formed a part of the Southern Ocean Gas Exchange Experiment (SOGEE)[15]. Very small bubbles with radii <60 μm were measured at 6–9 m water depth using optical measurements of near-forward volume scattering function and critical scattering angle.

A recent study describes a numerical model to estimate total bubble population for any spatial region in the ocean basin[16]. It parameterizes different stages of a microbubble assemblage underlying a wind-driven sea surface, and estimates the bubble population close to ocean surface. The estimated overall bubble population[16] takes into account different stages of bubble life, its geometrical aspect and spatial distribution. There are three categories of bubble clouds such as α, β and γ-plumes[17]. This categorization depends on bubble life expectancy during active bubble generation process in the ocean, driven by wind action on the sea surface. In a generic form, the bubble population model uses the population density spectrum level for each bubble assemblages[16]. It is a function of bubble radius, water depth, wind speed and shape function. The shape function depends on bubble plume and e-folding depth of bubble assemblages[16]. The bubble population density model[16] used a generalized spectral shape function applicable for β- and γ-plumes. A case study in the work[16] dealt with bubble plumes for the central Arabian Sea that experienced strong winds and large-scale wave breaking, based on information from GEOSAT altimeter data[18]. The model used near real-time winds from the National Center for Atmospheric Research (NCAR), USA, as input, thereby computing the final estimates of bubble plumes and population[16]. The shape function governs the estimate of total bubble population, and comparison with measurements for near-surface bubble density under breaking waves showed a reasonably good match[19]. Unfortunately, limited research exists on oceanic bubbles in India's oceanographic sciences programme. Hence, there is a necessity to have more observational data on bubble population and e-folding depths to validate and fine-tune models. The bubble population model developed for the Indian seas[16] has inherent limitation representing the time dependence of bubble plume transition, and more oceanographic observational data in future can supplement in fine-tuning bubble population models.

In the open ocean, bubble clouds induced by wave breaking show a high degree of variability in both space and timescales. The void fractions can vary by an order of magnitude over a short time span. The bubble clouds so generated are quite inhomogeneous, and rapidly evolve through various physical processes such as bubble dissolution, degassing and advection by turbulent and coherent flows. No published work describes the long-range sound propagation through these real bubbles, due to limited observational data and knowledge gaps in the physics of bubble transition. The present work utilizes the results from bubble population model[16] to understand possible mechanism of acoustic scattering due to bubble plumes, and sound speed attenuation in the presence of bubble clouds. Further, statistical analysis investigates the attenuation coefficient of sound speed for random bubble population, with the objective to ascertain any specific or inherent trends in their probability distribution. The study also investigates bubble damping mechanism (effects from radiation, thermal and viscous damping) for bubble assemblages as a function of bubble size and acoustic frequency, with special emphasis on damping at resonance frequency. Thereafter, it investigates the role of bubble population and damping on attenuation coefficient and sound speed loss in a bubbly mixture. The study leads to the development of a canonical model with an intention to understand acoustic attenuation in the presence of gas bubbles at the air–sea interface.

The subsequent sections deal with damping associated with gas bubbles, attenuation effects due to bubbles, and statistical measure on sound speed attenuation under random bubbles, and followed by summary and conclusion in the last section.

Damping due to bubbles

Physics of damping due to bubbles

Bubbles excited to volume pulsations have a polytrophic equation of state for the enclosed gas that results in a phase difference between the change in pressure per unit original pressure and change in volume per unit original volume. Therefore, the work done in compressing the bubble is more than the work done by the bubble in expanding. This difference in the work done represents a net flow of heat energy into the liquid. Pulsating bubbles expend a portion of their energy in the form of spherical sound waves. The radiation damping is this loss of energy. For pulsating bubbles in an incompressible viscous fluid, the effect of viscosity is addressed through stress equations and the boundary conditions, rather than the Navier–Stokes equation of motion. At the bubble surface, there are viscous forces acting which exert excess pressure resulting in the dissipation of energy. In practice, the other causes of damping are usually more important than radiation damping (δ_r), and in particular, there is thermal damping (δ_t). There are additional but smaller effects due to the shear viscosity in water (δ_v). Experimental

results verify that the damping at resonance is due to thermal, radiation and possibly viscous damping[20].

A few widely dispersed bubbles, which are so small as to be invisible, can have an appreciable acoustic effect. When a large number of these small bubbles are present, the liquid will be nearly opaque acoustically. Small impurities in liquids, such as suspended particles, have negligible influence in comparison with increased damping due to bubbles. Therefore, bubbles are considerably important in the transmission of underwater sound. In order to understand the attenuation of sound by gas bubbles in liquids, knowledge on the fundamental processes by which pulsating bubbles dissipate their energy is required. The subsequent section presents a theoretical discussion on the fundamental processes by which pulsating gas bubbles in liquids dissipate their energy. The survey is limited to the case where amplitude of the volume pulsations assumes sufficiently small value such that pulsations described by linear equations are valid. The total damping is described by losses primarily originating from three processes[20], viz. (a) thermal damping attributed from thermal conduction between gas in the bubble and the surrounding liquid, (b) sound radiation damping, and (c) viscous damping due to viscous forces at the gas–liquid interface.

Radiation damping due to bubbles

In a compressible fluid, bubble excited into volume pulsations expends a portion of its energy by radiating spherical sound waves. The bubble is considered as a simple sound source; the bubble radius a is considered small compared to the wavelength λ of the radiated sound. For large-sized bubbles, the radiation damping constant at resonance is independent of frequency, and in terms of acoustic wave number k is expressed as[21]

$$\delta_{\text{radiation}} = ka. \tag{1}$$

Thermal damping due to bubbles

In this case, there is just as much heat flowing outward from the bubble during compression as the flow inward during expansion. The work done by driving pressure in compressing the gas space is just equal to the work done by expanding gas in moving the surrounding liquid. Therefore, the thermal process is polytropic for a real bubble, and a phase difference exists between the increase in pressure per unit original pressure and the decrease in volume per unit original volume. This phase difference can lead to a 'hysteresis' effect[8]. The work done on gas volume by the driving pressure during compression is more than the work done by the gas space in moving the surrounding liquid during expansion. This difference in the work done represents a net flow of heat into the liquid characterized by thermal damping. When driving pressure at the bubble surface compresses the bubble, there is work done on the gas space. This increases the internal energy, resulting in a transfer of heat energy through the gas. The added heat transfers by conduction from the gas bubble into the surrounding liquid.

The damping constant is given in terms of the dissipation coefficients (b and d are non-dimensional numbers representing real and imaginary components of the complex ratio of specific heat), corrected breathing frequency f_{R} and the given sound frequency f. The thermal damping constant is expressed in the form[21]

$$\delta_{\text{thermal}} = \left(\frac{d}{b}\right)\left(\frac{f_{\text{R}}}{f}\right)^2. \tag{2}$$

Viscous damping due to bubbles

In the presence of viscosity, there is transfer of momentum from one region of the liquid to another moving at a different velocity. Liquid element moving rapidly in a particular direction tends to transmit its momentum to other elements of the liquid. When a bubble expands, the small liquid element distorts; the radial thickness decreases while the lateral dimension increases. Likewise, when a bubble contracts, the liquid element distorts; now the radial thickness increases and the lateral dimension decreases. Since the liquid is incompressible, the cause of distortion is not by a change in the volume of the liquid element, but by viscous stresses. Consequently, more energy is required to compress the bubble than is regained in the subsequent expansion. The viscous damping constant in terms of the dynamic coefficient of shear viscosity (μ), angular frequency (ω), radius (a) and ambient density of fluid surrounding the bubble (ρ_{A}) is expressed as[21]

$$\delta_{\text{viscous}} = \frac{4\mu}{\rho_{\text{A}}\omega a^2}. \tag{3}$$

As discussed earlier, these three components completely add up to the total damping caused by the bubbles. Hence, the total damping constant is expressed as

$$\delta = \delta_{\text{radiation}} + \delta_{\text{thermal}} + \delta_{\text{viscous}}. \tag{4}$$

Damping at resonance

The bubble behaves as a simple damped oscillating system with one degree of freedom. Therefore, the differential equation of motion for the bubble system has the same form as the second-order linear differential equation for a mass fastened to a spring. As the bubble periodically

expands and contracts, the surrounding liquid is the inert mass set into vibration, while the stiffness is due to the gas in the bubble. In this case, the bubble breathing frequency (f_b) is expressed in the form

$$f_b = \frac{1}{2\pi a}\sqrt{\frac{3\gamma P_A}{\rho_A}}, \tag{5}$$

where a is the mean radius of the bubble, P_A the static pressure corresponding to bubble mean radius, γ the ratio of the specific heats of the gas enclosed in the bubble and ρ_A is the ambient fluid density. Considering that $P_A = P_{atm}\,(1 + 0.4z)$ for bubble at the ocean surface, bubble breathing frequency in terms of water depth (z) is[21]

$$f_b = \frac{3.25\times 10^6}{a(\mu\text{m})}\sqrt{1+0.1z}. \tag{6}$$

Frequency correction due to thermal damping

It is evident from the above discussion that thermal damping is the most prominent component for total damping due to bubbles; there is a need to correct the bubble breathing frequency in order to get the bubble resonance frequency. To correct f_b due to thermal effects, the resonance frequency of the bubble f_R is defined in terms of average interior pressure (P_{int}) that depends on surface tension: $P_{int} = \beta P_A$ (where β is the ratio of bubble interior pressure to ambient pressure), and the effective ratio of specific heats that depends on thermal conductivity, γb (where γ is the ratio of specific heats of the gas). Here, γ in terms of real (b) and imaginary (d) components of the complex ratio of specific heats can be related by the complex expression $\gamma(b + id)$. The relation between bubble breathing frequency and resonance frequency is expressed as[21]

$$f_R = f_b\sqrt{b\beta}. \tag{7}$$

In the present study, solutions are obtained by computing equations (8)–(11) below in sequence[21]

$$X = a\left(\frac{2\omega\rho_g C_{pg}}{K_g}\right)^{1/2}, \tag{8}$$

$$\frac{d}{b} = 3(\gamma-1)$$

$$\times\left[\frac{X(\sinh X+\sin X)-2(\cosh X-\cos X)}{X^2(\cosh X-\cos X)+3(\gamma-1)X(\sinh X-\sin X)}\right], \tag{9}$$

$$b^{-1} = \left[1+\left(\frac{d}{b}\right)^2\right]\left[1+3(\gamma-1)\frac{(\sinh X-\sin X)}{X(\cosh X-\cos X)}\right], \tag{10}$$

$$\beta = \frac{p_{int}}{p_A} = 1+\frac{2\tau}{\rho_A a}\left(1-\frac{1}{3\gamma b}\right). \tag{11}$$

The values of b and β obtained from eqs (10) and (11) can be used along with eqs (6) and (7) to get the corrected resonance frequency. Most of these constants are traditionally expressed[21] in CGS units. The bubble gas density $\rho_g = \rho_{gA}[1 + 2\tau/(p_A a)](1 + 0.1z)$, where z is the depth (m); p_A the ambient pressure = $1.013 \times 10^6 \times (1 + 0.1z)$ (dynes/cm^2); ρ_{gA} the density of free gas at sea level (1.29×10^{-3} g/cm^3); C_{pg} the specific heat at constant pressure of bubble gas (≈ 0.24 cal/g °C); K_g the thermal conductivity for gas bubbles (≈ 5.6×10^{-5} cal/cm s °C); γ the ratio of specific heats for gas bubbles (1.4 for air) and τ is the surface tension at the air–water interface (≈ 75 dyne/cm). The variation of b, β and f_R/f_b at resonance as a function of bubble radius at four sample frequencies of 5, 30, 60 and 100 kHz is shown in Figure 1. Further computations are made for the radiation, thermal and viscous damping constants at resonance for two sample frequencies 30 kHz and 100 kHz, after the necessary frequency correction. Figure 2 shows the damping constants as a function of resonant frequencies and bubble radius. It is evident from Figure 2 that the contribution of thermal damping towards total damping is the most prominent compared to radiation and viscous counterparts. The contribution of thermal damping is substantial for these sample frequencies, and slightly less than an order compared to the radiation and viscous damping. A similar observation of thermal damping is evident for varying bubble sizes.

Attenuation due to bubbles

When there exist bubbles of varying sizes, the extinction cross-section per unit volume, S_e, for sound traversing a random mixture of non-interacting bubbles in range $ka < 1$ is calculated using the following expression[21]

$$S_e = \int_0^\infty \frac{4\pi a^2(\delta/\delta_r)\{n(a)\mathrm{d}a\}}{[(f_R/f)^2-1]^2+\delta^2}, \tag{12}$$

where δ and δ_r are the respective non-dimensional damping constant of bubble and scattering effects, and $n(a)\mathrm{d}a$ is the number of bubbles with radius a in increment da per unit volume. Under the assumption that the energy absorbed by the bubbles per unit volume in the cavity is the same as in a travelling wave, the attenuation per unit distance (α), due to bubble population $n(a)$ follows the expression

$$\alpha = 4.34 S_e. \tag{13}$$

However, if the bubbles are assumed to be of the same size, then there is no requirement of integration over a

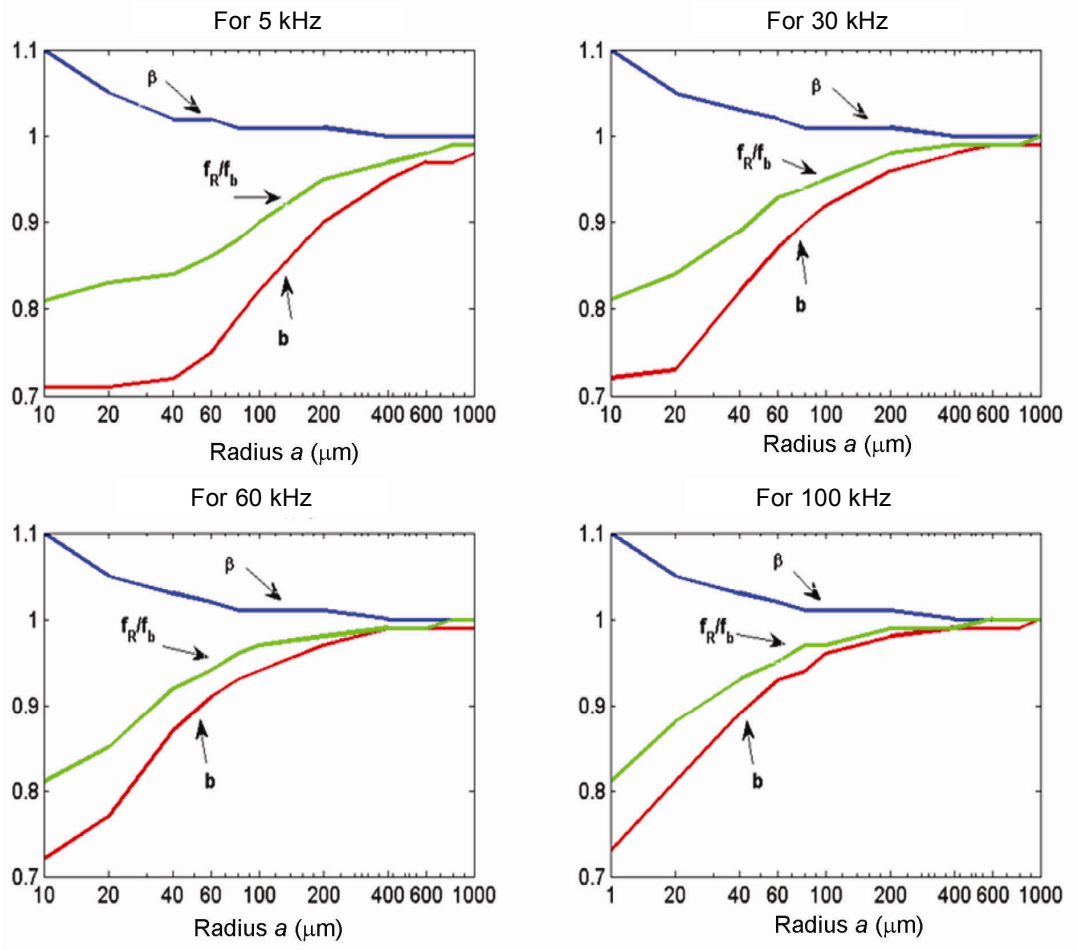

Figure 1. Variation of b, β and f_R/f_b at four sample frequencies – 5, 30, 60 and 100 kHz.

range of bubble radii and the attenuation coefficient can then be expressed in terms of total extinction cross-section (σ_e) as[21]

$$\alpha = 4.34\sigma_e N. \tag{14}$$

Sound speed dispersion relation

Extensive research work has been attempted to achieve a relationship that can predict sound speed attenuation in the presence of bubbles. The most notable work[22] states that sound speed in a compressible continuum is given by the bulk modulus (B) represented by the relation: $B = -V(\mathrm{d}p/\mathrm{d}V)$, where V is the ambient volume, dp the change in pressure and dV is the change in volume. Therefore, the sound speed is $c = (B/\rho)^{0.5}$, where ρ denotes the water density. In a bubbly mixture, the complex dispersion relation is[8]

$$\frac{C_0^2}{C_m^2} = 1 + 4\pi c_0^2 \int_0^\infty \frac{aN(a)}{\omega_0^2 - \omega^2 + \mathrm{i}\delta\omega^2}\,\mathrm{d}a, \tag{15}$$

where C_0 is the speed of sound in pure liquid, C_m the complex sound speed in the fluid with bubbles, a the bubble radius, ω the measurement frequency, ω_0 the natural frequency of a bubble, δ the bubble damping and $N(a)$ is the bubble density function within 1 μm radius range da centred at a. The bubble distribution approximates by a continuous field in which the medium acoustic properties are homogeneous in space. The influence of bubbles on both real and imaginary components of the sound speed can be obtained[21]. The real part represents the actual speed of sound in the bubbly medium, and the imaginary part represents the attenuation of sound waves by the bubbles

$$c_{\mathrm{real}} = C_0 \left\{ 1 - (2\pi c_0)^2 \int_{a_{\min}}^{a_{\max}} \frac{a}{\omega^2} \frac{[(\omega_0/\omega)^2 - 1]N(a)\mathrm{d}a}{\{[(\omega_0/\omega)^2 - 1]^2 + \delta^2\}} \right\}, \tag{16}$$

$$c_{\mathrm{imag}} = C_{\mathrm{real}} \left\{ \int_{a_{\min}}^{a_{\max}} \frac{2\pi a}{(\omega_0/c_0)^2} \frac{(\omega_0/\omega)^2 \delta N(a)\mathrm{d}a}{\{[(\omega_0/\omega)^2 - 1]^2 + \delta^2\}} \right\}. \tag{17}$$

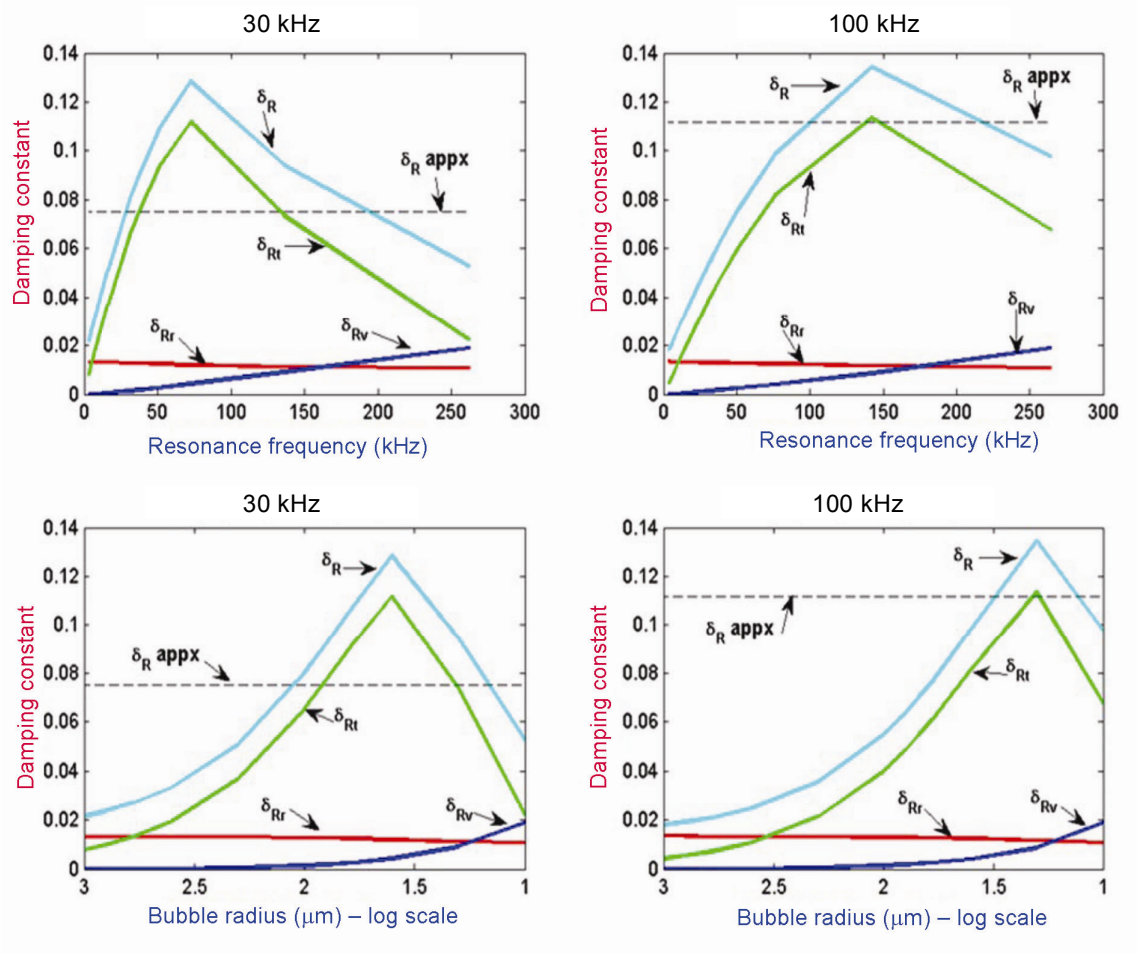

Figure 2. Variation of thermal, radiation and viscous damping for frequencies of 30 and 100 kHz for varying resonance frequency and bubble radius.

Results from bubble attenuation model

The segregation of oceanic bubble plumes depends on their maximum e-folding depth as well their lateral extent. Dense bubble plumes (with radius greater than 1 mm) exhibit significant population of larger bubbles and vice versa for the diffuse plumes[23]. The variability of sound speed propagation in a bubbly medium can be quite distinct. Based on measurements, the variability can be in the order of about 800 m s^{-1} at low frequencies for young bubble clouds in a short-time interval, to about 400 m s^{-1} for mature clouds located at e-folding depth ≈0.5 m below the sea surface[19]. As mentioned above, the bubble population model used in the study by Saxena and Prasad Kumar[16] parameterizes the overall bubble population for different stages of bubble life, as well as their geometrical aspect and spatial distribution. The penetration depth (d) expressed as a function of wind speed measured at a height of 10 m above sea surface and used in the present study is expressed in the form[24]

$$d = 0.4(U_{10} - 2.5), \tag{18}$$

where U_{10} is wind magnitude at a height of 10 m above the sea surface expressed (m s^{-1}). Experiments conducted in the open sea at Oban[25] reported that long swells have an important effect on the formation of sporadic bubble cloud patches in open water. Based on this work[25], the largest bubble (having size r) carried down by the action of wind on the sea surface is expressed as

$$r = 26.7U_{10}^{1/2}. \tag{19}$$

Equation (19) is a thumb-rule formula to get an approximate size for bubbles as a function of wind speed. In a mathematical sense, the population density spectrum level for each bubble assemblage is expressed in a generic functional form[26] as

$$P(a, z, w) = N_0 G(a, z) Z(z, w) U(w), \tag{20}$$

where a is the bubble radius, z the water depth; U the wind-dependent factor to estimate the bubble population density, a function of wind speed (w) at a reference height of 10 m above sea surface; N_0 a constant that

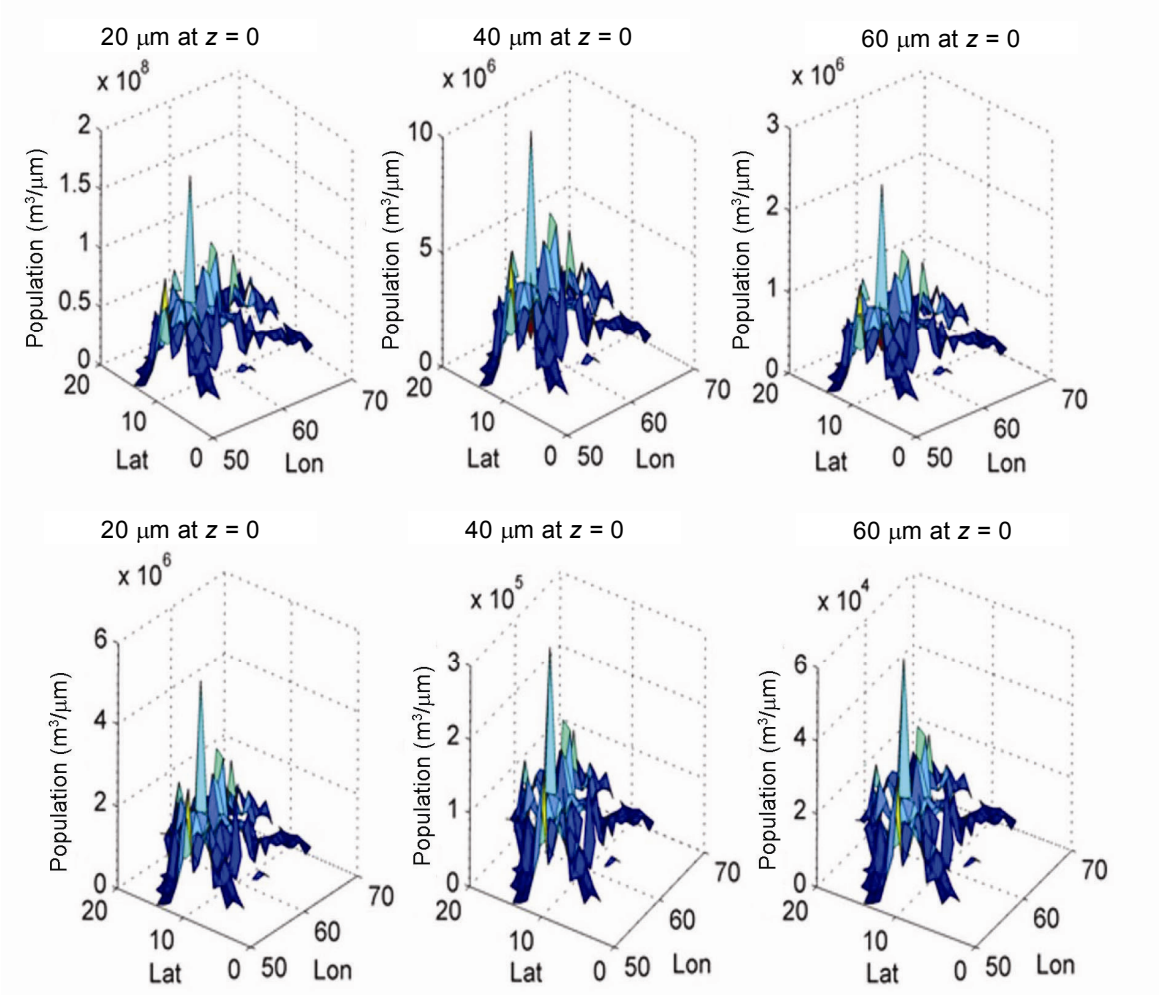

Figure 3. Spatial variability of total bubble population. (Top panel) β-plume and (Bottom panel) γ-plume for bubble sizes of 20, 40 and 60 μm at sea surface.

refers to the value of P at a reference radius, depth and wind speed condition; $G(a, z)$ is the shape function related to bubble plume and $Z(z, w)$ is a depth-dependent function that basically signify the e-folding depth characteristics. As the e-folding depth for various bubble plumes is standardized with reference to the sea surface ($z = 0$), the general form of population density spectrum level given in eq. (20) can be expressed as

$$P(a, z, w) = N_0 G(a) Z(z) U(w). \quad (21)$$

A generalized spectral shape function $G(a)$ verified for the central Arabian Sea[16] and used for the present study accounts all bubble assemblages such as β-, γ-plumes and background bubble layer expressed in the form[16]

$$G(a) = \begin{cases} 0, & \text{for } a < a_{\min} \\ (a/a_1)^3, & \text{for } a_{\min} \le a < a_1 \\ 1, & \text{for } a_1 \le a \ge a_2 \\ (a_2/a)^4, & \text{for } a_2 < a \le a_3. \end{cases} \quad (22)$$

Figure 3 shows the spatial variability of model-computed bubble populations[16] for β- and γ-plumes for sizes 20, 40 and 60 μm at sea surface in the central Arabian Sea.

In the present study, the attenuation due to bubbles is estimated from eqs (13) and (16) using inputs from the bubble population model $N(a)$ and δ from the bubble damping model. Figure 4 shows the variation of sound-speed attenuation rate α (expressed in dB/m) in the presence of bubbles at two different wind speeds of 12 and 15 m s^{-1} for the frequency range from 5 to 100 kHz. Higher attenuation rates occur when wind speed increases from 12 to 15 m s^{-1}. Frequencies in excess of 45 kHz experience a drastic increased attenuation, reaching threshold maxima around 90 kHz, and declining thereafter. In a physical sense, the attenuation increases gradually with increasing frequency and the rise is rapid approaching the resonant frequency. Attenuation is high for higher frequencies compared to lower frequencies. Beyond resonance, the attenuation decreases gradually. Therefore, the dependence of resonant frequency is inversely proportional to the bubble radius. For a range of

fractional air volume, the attenuation increases at a rate approximately proportional to the square root of the bubble air volume. It is essentially due to heat conduction from pulsating bubbles below the resonant frequency, and sound scattering above the resonant frequency, wherein the viscous damping effects are not significant[27].

Having established the role of wind speed on variability of bubble attenuation rate, and to ascertain the total effect of bubbles on attenuation characteristics, the present study also investigates the sound speed variability for the central Arabian Sea basin. Figure 5 shows a flowchart of the damping model and the associated modules. The precomputed scenarios for total bubble population in the central Arabian Sea were available[16], and this justifies the selection of the region. Two case studies are performed to determine sound speed attenuation, viz. on bubble-free water and in the presence of bubbles. The essential inputs to estimate sound speed (temperature, salinity and water depth) comprise data from the Levitus World Ocean Atlas (WOA). The WOA is a product from Ocean Climate Laboratory of National Oceanographic Data Center, USA. It contains climatology fields of temperature and salinity fields at different vertical levels for the global oceans. The datasets from WOA are an objective analysed product available on global scale at a grid resolution of 1° × 1°. This study uses the representative month of July, as during the southwest monsoon season, winds are quite strong in the central Arabian Sea with pronounced wave-breaking activity. The sound speed relation uses the equation[28] as follows

$$C(T, S, z) = a_1 + a_2T + a_3T^2 + a_4T^3 + a_5(S - 35) + a_6z + a_7z^2 + a_8T(S - 35) + a_9Tz^3, \quad (23)$$

where T, S and z are the fields of temperature (°C), salinity (ppt), and depth (m) respectively. The constants $a_1, a_2, \ldots, a_9$ in eq. (23) are given by[28]

$$a_1 = 1448.96;\ a_2 = 4.591;\ a_3 = -5.304 \times 10^{-2};$$
$$a_4 = 2.374 \times 10^{-4};\ a_5 = 1.340;\ a_6 = 1.630 \times 10^{-2};$$
$$a_7 = 1.675 \times 10^{-7};\ a_8 = -1.025 \times 10^{-2};$$
$$a_9 = -7.139 \times 10^{-13}.$$

The sound speed estimate for bubble-free water using eq. (23) provides the quantity C_0 (speed of sound in pure liquid without bubbles) shown in eq. (16). Using this estimated value of C_0, calculations for the variable c_{real} containing the damping term provide the sound speed characteristics in the presence of bubbles. A comparison of the sound speed characteristics at two different locations in the central Arabian Sea (12°N; 67°E and 12°N; 53°E), a region that experienced high wind speeds, is shown in Figure 6. It is clear that bubble effects dominate the sound speed characteristics until depth levels of approximately 6–7 m below the water surface. The estimated loss in sound speed is about 30–45 m s^{-1} due to the presence of bubbles at the sea surface.

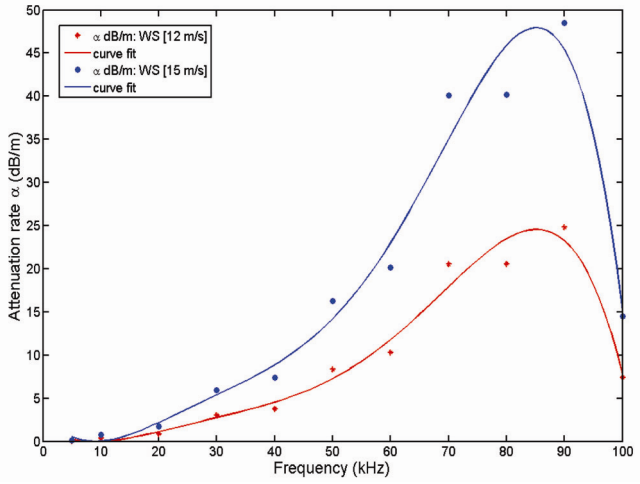

Figure 4. Variation of attenuation rate with resonance frequency for wind speed (ws) of 12 and 15 ms^{-1}.

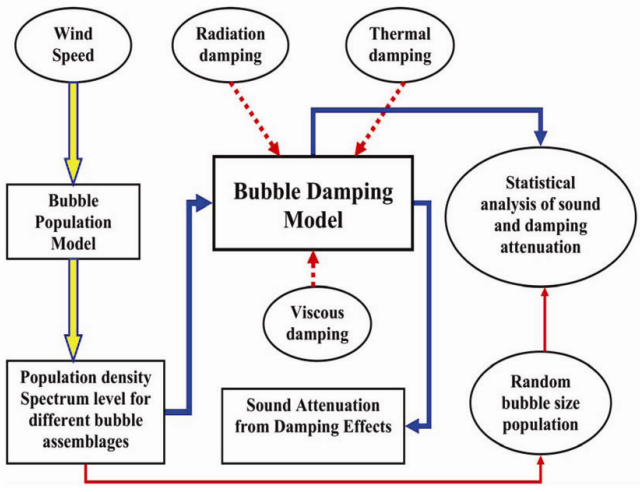

Figure 5. Flowchart of the damping model.

Statistical analysis

The bubble population model at any point of time provides the maximum number of bubbles/m^3 for a given radius and wind speed. Real sea state contains varying number of bubbles having different size and population; therefore, a statistical analysis of its distribution will be useful in acoustic applications. In addition, the recordings for actual bubble population are scanty, and their probability of occurrence of any given size is unknown. Therefore, the knowledge of its statistical distribution can aid population models to have realistic estimate of attenuation. In this study, an attempt was made to generate random bubble size population with calculated c_{real} and α values, and thereby understand whether inherent

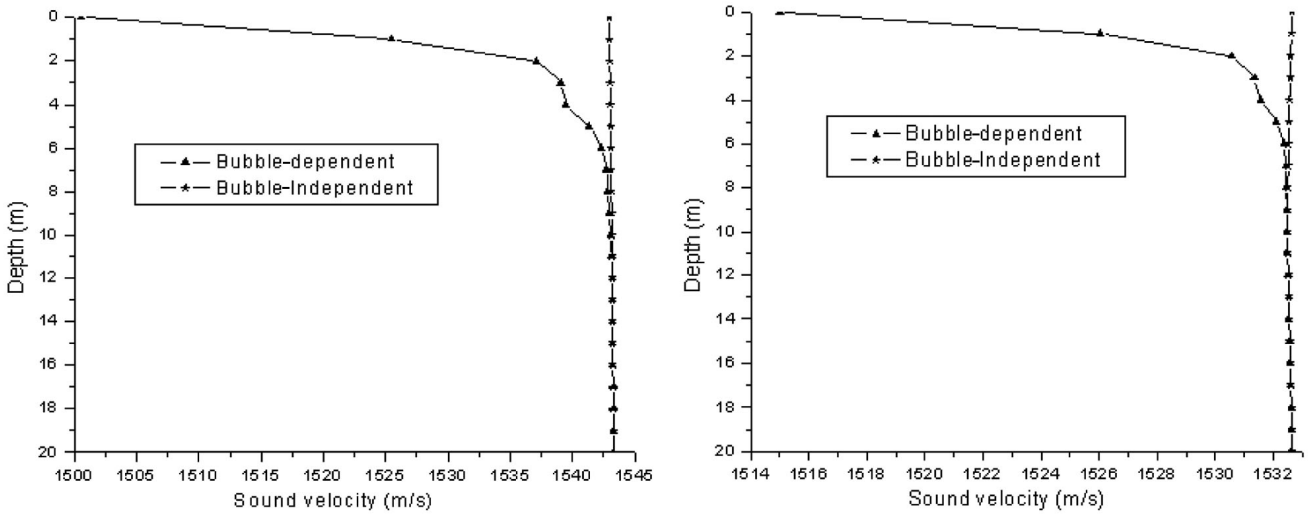

Figure 6. Sound speed profile (m s^{-1}) in the presence and absence of bubbles at geographical locations 12°N, 67°E (top panel) and 12°N, 53°E (bottom panel).

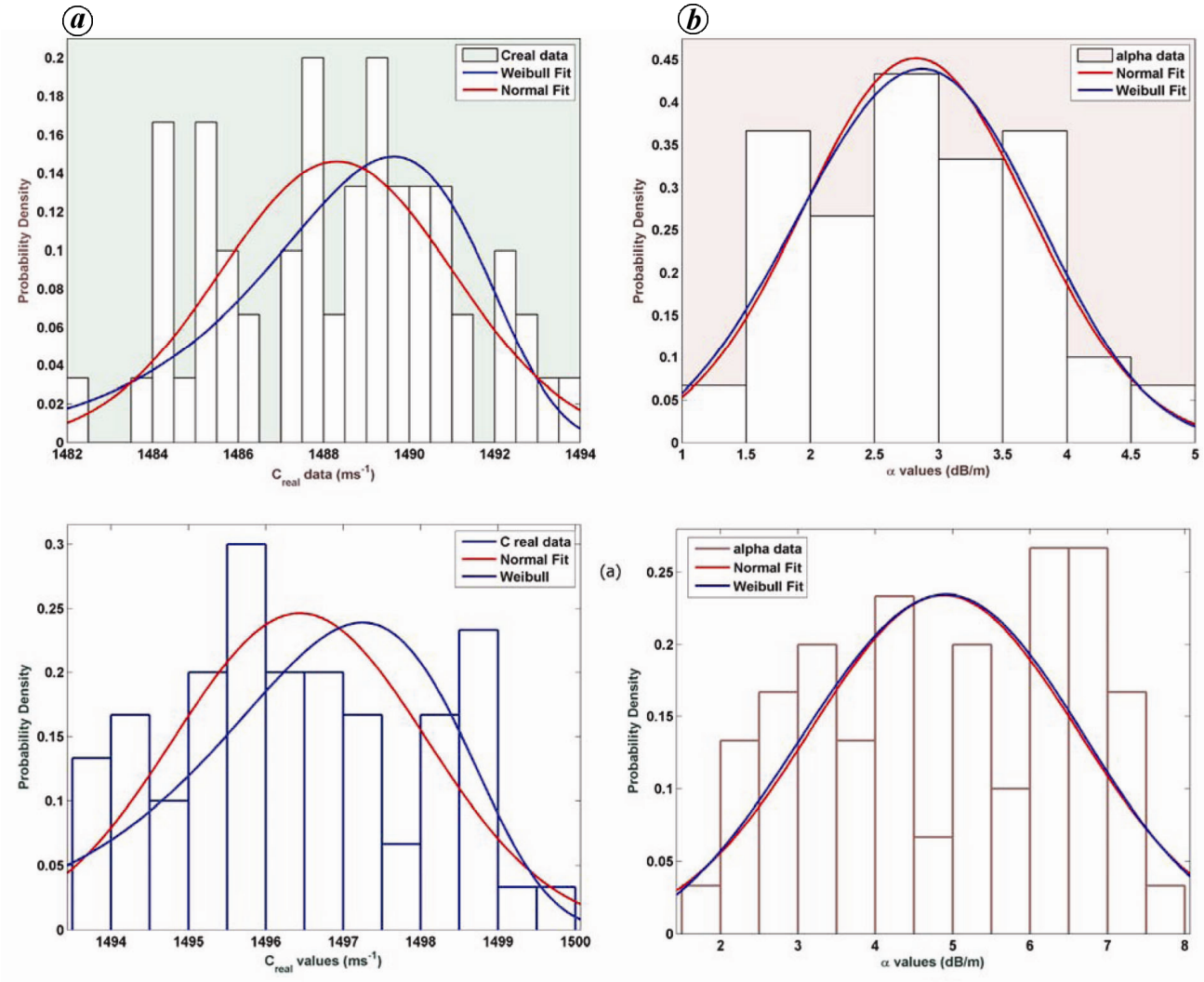

Figure 7. Statistical distribution fit of attenuation coefficient and real sound speed for (***a***) wind speed 15 m s^{-1} and input frequency 30 kHz and (***b***) wind speed 12 m s^{-1} and input frequency 60 kHz.

trends such as Gaussian, Weibull, exponential, lognormal or any other well-known patterns exist. The fitting of a theoretical distribution is a three-step process involved in identifying candidate distribution, estimating the parameters and performing the goodness-of-fit test[29]. This study performs analysis of 60 samples for c_{real} and α values using 12 and 15 m s^{-1} wind speed, with corresponding frequencies of 60 and 30 kHz. If this random c_{real} and α estimate had a symmetrical or near-symmetrical distribution, such as normal or a Weibull with shape parameter between 3 and 4, then the sample mean and median values will be approximately equal. When mean is considerably larger than median, the data are skewed to the right and the exponential, lognormal or Weibull will provide a better fit. For exponential distribution, the sample mean and standard deviation must be approximately equal. The results signify that the mean and median values were approximately equal, denoting that normal distribution is a good fit. The probability density and fit distributions are shown in Figure 7 *a* and *b* respectively. The goodness-of-fit determines the selection of a suitable theoretical distribution. The sample statistics compared with the critical value suggest that in case the test statistics is less than the critical value, the hypothesis is accepted. The results signify that the sample data more or less follow the normal distribution and the test for goodness of fit is the Kolmogorov–Smirnov test. It compares the maximum deviation between empirical cumulative distribution and hypothesized cumulative distribution[30]. This study performs the test for a significance level of 0.05 and the hypothesis was accepted. It deciphers the fact that even though bubble generation process is completely random in nature, the distribution of sound speed characteristics and attenuation is not fully random; rather it follows a normal distribution. The findings of this result is a hypothesis based on statistical test; however, the real probability distribution requires a comprehensive field programme on bubble population measurement in the open sea.

Summary and conclusion

The potential generation of near-surface oceanic gas bubbles is primarily due to breaking waves when a threshold limit of wind speed is expected. The bubble clouds generated are nonlinear in both space and timescales. The cloudy aspect of the bubble layer introduces, de facto, range dependence in both acoustic propagation and attenuation characteristics. At present there are scanty observations on bubble population, and inherent complexity is involved in modelling plume evolution. As a first approximation, acousticians treat the bubbly environment as homogenous in range, and occasionally in vertical scales. Therefore, a novel technique to understand bubble population and modelling its spatial and temporal variability is needed to improve the capability in underwater sound propagation. Recently, a model that determines the spatial distribution of bubble population was developed for the central Arabian Sea for high wind conditions and wave breaking activity. It considered the southwest monsoon period prone to significant wave heights in the order of 5–7 m. The threshold wind speeds during this period were amicable to generate quasi-periodic wave-breaking regimes and bubble generation. The population model parameterizes bubble distribution at different stages of its evolution considering the geometrical aspects. In this study we have developed a damping model that considers the cumulative effects from radiation, shear viscosity and thermal conductivity using inputs from the population model. It has inherent freedom in estimating perturbation of sound speed and excess attenuation in the presence of bubbles having varying population and sizes. Subsequent to the development of population and damping model, the study investigates the random nature of bubble concentration. The objective was to develop a suitable statistical distribution function for sound speed propagation and damping characteristics. In this context, numerous numerical experiments were performed for different e-folding depths, foam patch size and spacing between plumes to estimate the statistical distribution function. The results signify that both damping and sound speed characteristics more or less follow a normal distribution. Finally, the study advocates that there is a need to conduct numerous field campaigns on bubble measurements to fine-tune the numerical model, having the potential to develop a single canonical bubble spectrum model for underwater acoustics.

1. Kolovayev, D. A., Investigation of the concentration and statistical size distribution of wind-produced bubbles in the near-surface ocean. *Oceanology (English Transl.)*, 1976, **15**, 659–661.
2. Medwin, H., *In situ* acoustic measurements of microbubbles at sea. *J. Geophys. Res.*, 1977, **82**, 971–975.
3. Johnson, B. D. and Cooke, R. C., Bubble populations and spectra in coastal waters: a photographic approach. *J. Geophys. Res.*, 1979, **84**, 3761–3766.
4. Walsh, A. L. and Mulhearn, P. J., Photographic measurements of bubble populations from breaking waves at sea. *J. Geophys. Res.*, 1987, **92**, 14553–14565.
5. Farmer, D. M. and Vagle, S., Waveguide propagation of ambient sound in the ocean surface bubble layer. *J. Acoust. Soc. Am.*, 1989, **86**, 1897–1908.
6. Breitz, N. and Medwin, H., Instrumentation for *in situ* acoustical measurements of bubble spectra under breaking waves. *J. Acoust. Soc. Am.*, 1989, **86**, 739–743.
7. Farmer, D. M. and Vagle, S., Bubble measurements using a resonator system. In *Natural Physical Processes Associated with Sea Surface Sound* (ed. Leighton, T. G.), University of Southampton, UK, 1997, pp. 155–162.
8. Leighton, T. G., *The Acoustic Bubble*, Academic Press, London, 1994, pp. 613.
9. Newhouse, V. L. and Shankar, P. M., Bubble sizing using the nonlinear mixing of two frequencies. *J. Acoust. Soc. Am.*, 1984, **75**, 1473–1477.

10. Chapelon, J. Y., Shankar, P. M. and Newhouse, V. L., Ultrasonic measurement of bubble cloud size profiles. *J. Acoust. Soc. Am*., 1985, **78**, 196–201.
11. Shankar, P. M., Chapelon, J. Y. and Newhouse, V. L., Fluid pressure measurement using bubbles insonified by two frequencies. *Ultrasonics*, 1986, **24**, 333–336.
12. Koller, D., Li, Y., Shankar, P. M. and Newhouse, V. L., High speed bubble sizing using the double frequency technique for oceanographic applications. *IEEE J. Ocean. Eng*., 1992, **17**, 288–291.
13. Phelps, A. D., Ramble, D. G. and Leighton, T. G., The use of a combination frequency technique to measure the surf zone bubble population. *J. Acoust. Soc. Am*., 1997, **101**, 1981–1989.
14. Phelps, A. D. and Leighton, T. G., Oceanic bubble population measurements using a buoy-deployed combination frequency technique. *IEEE J. Ocean. Eng*., 1998, **23**, 400–410.
15. Randolph, K., Dierssen, H. M., Twardowski, M., Lorenzen, A. C. and Zappa, C. J., Optical measurements of small deeply penetrating bubble populations generated by breaking waves in the Southern Ocean. *J. Geophys. Res*., 2014, **119**, 757–776.
16. Saxena, U. and Prasad Kumar, B., A bubble population density spectrum model for the central Arabian Sea. *J. Ship Technol*., 2010, **6**, 30–44.
17. Monahan, E. C. and Lu, M., Acoustically relevant bubble assemblages and their dependence on meteorological parameters. *IEEE J. Ocean. Eng*., 1990, **15**, 340–349.
18. Vethamony, P. *et al.*, Wind and wave climatology for Indian Ocean from GEOSAT altimeter. NIO Technical Report, NIO, Goa, 2000, pp. 1–31.
19. Novarini, J. C., Keiffer, R. S. and Norton, G. V., A model for variations in the range and depth dependence of the sound speed and attenuation induced by bubble clounds under wind-driven sea surfaces. *IEEE J. Ocean. Eng*., 1998, **23**, 423–438.
20. Charles Jr, D., Survey of thermal, radiation, and viscous damping of pulsating air bubbles in water. *J. Acoust. Soc. Am*., 1959, **31**, 1654–1667.
21. Medwin, H. and Clay, C. S., *Fundamentals of Acoustical Oceanography*, Academic Press, New York, 1998, p. 712.
22. Farmer, D. M., Vagle, S. and Booth, A. D., A free-flooding acoustical resonator for measurements of bubble size distributions. *J. Atmos. Ocean. Technol*., 1998, **15**, 1132–1146.
23. Leifer, I., Caulliez, G. and Leeuw, G. D., Characteristics of bubble plumes, bubble plume bubbles and waves from wind-steepened wave breaking. *J. Mar. Syst.*, 2007, **66**, 61–70.
24. Thorpe, S. A. and Stubbs, A. R., Bubbles in a freshwater lake. *Nature*, 1979, **279**, 403–405.
25. Thorpe, S. A., On the clouds of bubbles formed by breaking waves in deep water and their role in the air-sea gas transfer. *Philos. Trans. R. Soc. London, Ser. A*, 1982, **304**, 155–210.
26. Hall, M. V., A comprehensive model of wind-generated bubbles in the ocean and predictions of the effects on sounds propagation at frequencies up to 40 kHz. *J. Acoust. Soc. Am.*, 1989, **86**, 1103–1116.
27. Domenico, S. N., Acoustic wave propagation in air-bubble curtains in water – Part I: History and theory. *Geophysics*, 1982, **47**, 345–353.
28. MacKenzie, K. V., Discussion of seawater sound-speed determinations. *J. Acoust. Soc. Am*., 1981, **70**, 801–806.
29. Charles, E. E., *An Introduction to Reliability and Maintainability Engineering*, Waveland Press Inc, Illinois, 2005, p. 486.
30. Chakravarti, I. M., Laha, R. G. and Roy, J., *Handbook of Methods of Applied Statistics*, John Wiley, New York, 1967, p. 160.

Received 16 May 2014; revised accepted 8 July 2014